

Efficient optimization of state preparation in quantum networks using quantum trajectories

Michael H Goerz^{1,2}, Kurt Jacobs^{2,3,4}

E-mail: goerz@stanford.edu

¹Edward L. Ginzton Laboratory, Stanford University, Stanford, CA 94305, USA.

²U.S. Army Research Laboratory, Computational and Information Sciences Directorate, Adelphi, MD 20783, USA.

³Department of Physics, University of Massachusetts at Boston, Boston, MA 02125, USA

⁴Hearne Institute for Theoretical Physics, Louisiana State University, Baton Rouge, LA 70803, USA

Abstract. The wave-function Monte-Carlo method, also referred to as the use of “quantum-jump trajectories”, allows efficient simulation of open systems by independently tracking the evolution of many pure-state “trajectories”. This method is ideally suited to simulation by modern, highly parallel computers. Here we show that Krotov’s method of numerical optimal control, unlike others, can be modified in a simple way, so that it becomes fully parallel in the pure states without losing its effectiveness. This provides a highly efficient method for finding optimal control protocols for open quantum systems and networks. We apply this method to the problem of generating entangled states in a network consisting of systems coupled in a unidirectional chain. We show that due to the existence of a dark-state subspace in the network, nearly-optimal control protocols can be found for this problem by using only a single pure-state trajectory in the optimization, further increasing the efficiency.

Keywords: quantum optics, quantum networks, optimal control, numerical methods

1. Introduction

The control of simple quantum systems is central to the future realization of quantum technologies [1, 2, 3, 4]. Such systems are usually open, meaning that they experience a significant source of noise from their environments [5, 6]. Systems that form the nodes in a quantum network, in which the nodes are connected together via traveling-wave fields are also necessarily open due to the interaction with the fields. [6, 7, 8, 9] At the simplest level, open quantum systems and networks can be described by a first-order differential equation for the density matrix called a master equation. A useful feature of master equations is that the evolving density matrix for the system or systems can alternatively be written as the average over an ensemble of pure states in which the evolution of each state is given by an equation with a random (stochastic) component [10, 11, 12, 13, 6]. For a d -dimensional system the representation of the density matrix scales as d^2 while that of a pure state scales only as d . For this reason the pure-state ensemble approach, or “quantum trajectory” approach, can provide a significant reduction in numerical overhead. Here we use the trajectory method in which the stochastic element is a series of “jumps” at random times, often referred to as the “quantum Monte Carlo” or “quantum-jump trajectories” method [14, 15, 16].

The ability to vary one or more parameters of the Hamiltonian of a system over time is a powerful tool for controlling the system. The problem of determining the time-dependence, or “pulse shapes” required to realize a given evolution is highly non-trivial, however, and as a result numerical search methods, often referred to as “optimal control” methods, are very useful for this purpose [17, 18]. To perform a numerical search requires simulating the evolution of a system or network many times under differing pulse shapes to sufficiently explore the “control space” of possible pulses. The use of quantum trajectories for such simulations, especially as the size of a network increases, is thus desirable.

Here we examine the form that gradient-based numerical search methods take when written in terms of the ensemble of pure state evolutions (the “quantum trajectories”) that simulate the master equation. We show that unlike other methods, Krotov’s method can be formulated in such a way that updates to the pulse shapes are obtained either from independent trajectories, or by quadratic cross-referencing of trajectories. We then show via a numerical example that Krotov’s method remains effective even for a small number of trajectories, including a single trajectory.

In the second part of this work we apply the above “Krotov trajectory method” to a problem of preparing a class of entangled states in a simple network. This network consists of a “chain” of systems connected via a single unidirectional field. Each system, or “node” in the network is a cavity containing a system with two stable levels, and for which the interaction with the cavity mode can be turned on and off via a local control field. One way in which these nodes can be realized is by having a three-level atom in each cavity, in which the three levels are in a lambda configuration. The two ground states provide the two stable levels, and the interaction between these two levels and the cavity mode is mediated by an off-resonant coupling to the excited state. Our problem may be thought of as a generalization of the configuration used by Cirac *et al.* in their seminal work in which they showed how the state of a two-level system in a cavity could be transferred to a second two-level system in a second cavity via a unidirectional field [19]. They found that, so long as the coupling of each cavity to the traveling-wave field was the only source of dissipation, the coupling between the two-level systems and their respective cavities could be controlled in such

a way that the excitation stored in the first two-level system could be emitted into the field, enter the second cavity, and be completely re-absorbed by the second two-level system, without being lost from the second cavity to the outward-traveling field. Strictly speaking, to effect perfect transfer in this way requires an infinite time, since the transfer of the excitation to the field is an exponential decay, but near-unity fidelity can be obtained within a finite multiple of the decay time. One way to understand the protocol of Cirac *et al.* is to say that there is a subspace of joint states of the two nodes that are “dark” in the sense that no photons will be emitted from the systems when in this subspace [20, 21, 22, 23]. The protocol is able to realize the transfer by evolving exclusively within this subspace.

Here we consider the preparation of Dicke states of N nodes in which a single excitation, originally prepared in the first node, is shared equally between all the nodes. We find that by controlling only the local coupling between the nodes and the field link it is possible to prepare these multi-partite entangled states while remaining within the dark-state subspace, thus realizing essentially perfect preparation (up to the finite duration of the protocol and any losses additional to the field link). We also find that because the optimal protocols are able to enter the dark-state subspace quickly on the timescale of the transfer, the majority of the numerical search can be performed with a single pure-state trajectory, thus greatly increasing the efficiency.

The rest of this paper is structured as follows. In Section 2 we first review the Monte-Carlo wavefunction method and the gradient-based GRAPE and Krotov optimization methods. Then, in Section 2.3, we develop the central result of this paper, a trajectory-based variant of Krotov’s method. We illustrate the method in a numerical case study in Section 3. We first introduce the network, model for a chain of cavities containing trapped atoms. Then, in Sections 3.2–3.4, we present the result of applying optimal control to the creation of a Dicke state in that system, and analyze the convergence and the noise properties of the optimized pulses. Section 4 concludes.

2. Optimal Control via Quantum Trajectories

2.1. The Monte-Carlo Wavefunction method

We consider the problem of initializing a quantum network from a well-defined separable state $|\Psi(t=0)\rangle$ to a (generally entangled) state $|\Psi_{\text{tgt}}(t=T)\rangle$. The network is characterized by a Hamiltonian $\hat{H} = \hat{H}_0 + \sum_i u_i(t)\hat{H}_i$ with one or more control fields $u_i(t)$, and a set of Lindblad operators $\{\hat{L}_l\}$ to describe dissipative processes. The dynamical map $\hat{\rho}(t) = \mathcal{E}(t,0)\hat{\rho}(0)$ denotes the solution of the Lindblad-von-Neumann equation

$$\frac{\partial \hat{\rho}}{\partial t} = -\frac{i}{\hbar} \mathcal{L} \hat{\rho} = -\frac{i}{\hbar} \left[\hat{H}(\{u_i(t)\}), \hat{\rho} \right] + \mathcal{L}_D \hat{\rho} \quad (1)$$

with the boundary condition $\hat{\rho}_0 = |\Psi(0)\rangle\langle\Psi(0)|$ and the dissipator \mathcal{L}_D .

For any network consisting of more than a trivially small number of nodes, the exponential growth of the Hilbert space will quickly render the numerical treatment of the system dynamics in Liouville space unfeasible. Significantly less resources are required to simulate the dynamics through quantum trajectories. In this case, $\hat{\rho}(t)$ is

approximated as an average of the pure states $|\Psi_k(t)\rangle\langle\Psi_k(t)|$ resulting from $M \rightarrow \infty$ trajectories indexed by k .

$$\rho(\hat{\mathbf{t}}) = \lim_{M \rightarrow \infty} \sum_k |\Psi_k(t)\rangle\langle\Psi_k(t)| \quad (2)$$

Each trajectory $|\Psi_k(t)\rangle$ is a possible, statistically independent, pure-state realization of the system dynamics, taking into account dissipative processes. There are several ways to obtain the trajectories, corresponding to different physical measurements on the environment, i. e., the intercavity field, and governed by different equations of motion. Measurements of one or both of the quadratures of the field result in a quantum diffusion equation (QSDE) [24], while photon counting results in quantum jumps (MCWF) [15, 16]. Since we are only interested in the average of (5), all of these are equivalent, and we will focus on the quantum jump method, as it is the most straightforward to realize numerically.

The *MCWF algorithm* for propagating the trajectory state $|\Psi_k\rangle$ is [25]

- 1: define the non-Hermitian effective Hamiltonian

$$\hat{H}_{\text{eff}} = \hat{H} + \sum_l \hat{L}_l^\dagger \hat{L}_l \quad (3)$$

- 2: draw a random number $r \in [0, 1)$
- 3: propagate until $|\Psi_k(t)|^2 = r$.
- 4: apply an instantaneous quantum jump

$$|\Psi_k(t)\rangle \rightarrow \frac{\hat{L}_l |\Psi_k(t)\rangle}{|\hat{L}_l |\Psi_k(t)\rangle|}$$

choosing \hat{L}_l from the set of all Lindblad operators with probability

$$p(\hat{L}_l) = \langle \Psi_k(t) | \hat{L}_l^\dagger \hat{L}_l | \Psi_k(t) \rangle \quad (4)$$

- 5: draw a new random number $r \in [0, 1)$ and continue the propagation.
- 6: normalize any resulting $|\Psi_k(t)\rangle$

2.2. Optimal Control with GRAPE and Krotov's method

We seek optimal solutions $u_i(t)$ to minimize the error functional

$$J_T = 1 - \langle\langle \hat{\rho}(T) | \hat{P}_{\text{tgt}} \rangle\rangle, \quad (5)$$

for a fixed duration T , where \hat{P}_{tgt} is the projector onto the target state $|\Psi_{\text{tgt}}\rangle$. We use the notation $\langle\langle a|b \rangle\rangle \equiv \text{tr}[a^\dagger b]$ for the Hilbert-Schmidt overlap of two operators.

There are well-established gradient-based methods of numerical optimal control to solve this problem. The two preeminent ones are Gradient-Ascent-Pulse-Engineering (GRAPE) [26], usually as a quasi-Newton method in combination with the L-BFGS-B algorithm [27, 28], and Krotov's method [29, 30, 31]. Both of these are *iterative*: They start from “guess” fields $u_i^{(0)}(t)$ and calculate updates $\Delta u_i(t) = u_i^{(1)}(t) - u_i^{(0)}(t)$ that decrease the value of the target functional; for the next iteration, $u_i^{(1)}$ becomes the guess, and the procedure repeats until convergence is reached.

The GRAPE method starts with the assumption that $u_i(t)$ with $t \in [0, T]$ is discretized into n_t time steps, such that the time evolution up to a point t_j is

$$\hat{\rho}(t_j) = \mathcal{E}(t_j, 0) \hat{\rho}(0) = \left(\prod_{j'=t_j}^1 \mathcal{E}_{j'} \right) \hat{\rho}(0) \quad (6)$$

where $\mathcal{E}_j \equiv \mathcal{E}(t_j, t_{j-1})$ denotes the dynamical map $\hat{\rho}(t_{j-1}) \rightarrow \hat{\rho}(t_j)$, with $t_0 = 0$ and $t_{n_t} = T$. The control fields are approximated as constant within the time interval, $u_{ij} \equiv u_i([t_{j-1}, t_j])$. Each time-local value $u_{ij}^{(0)}$ is modified according to the gradient,

$$\Delta u_{ij} \propto \frac{\partial J_T}{\partial u_{ij}} = -\left\langle\left\langle \hat{\rho}^{(0)}(t_j) \left| \frac{\partial \mathcal{E}_j}{\partial u_{ij}} \right| \hat{\rho}^{(0)}(t_{j-1}) \right\rangle\right\rangle, \quad (7)$$

where

$$\hat{\rho}^{(0)}(t_j) = \left(\prod_{j'=j+1}^{n_t} \mathcal{E}_{j'}^{(0)\dagger} \right) \hat{\rho}_{\text{tgt}} \quad (8)$$

is the target state backward-propagated with the conjugate Lindbladian. The superscript zero indicates the dynamics under the guess controls.

Krotov's method takes a slightly different approach. Starting from time-continuous guess controls $u_i^{(0)}(t)$, it analytically constructs pulse updates $\Delta u_i(t)$ that *globally* minimize an extended functional, commonly

$$J = J_T + \sum_i \frac{\lambda_i}{S_i(t)} \int_0^T \underbrace{[u_i^{(1)}(t) - u_i^{(0)}(t)]^2}_{=\Delta u_i(t)} dt, \quad (9)$$

where λ_i is an arbitrary weight determining the overall magnitude of $\Delta u_i(t)$, and $S_i(t) \in [0, 1]$ is a shape function that may be used to enforce boundary conditions. As the optimization converges, $\Delta u_i(t) \rightarrow 0$, such that J and J_T become equivalent. Note that the updated controls $u_i^{(1)}(t)$ are global minima only with respect to the specific guess $u_i^{(0)}(t)$ that appears explicitly in (9), not the overall search space. The control problem is solved by the update equation

$$\Delta u_i(t) = \frac{S_i(t)}{\lambda_i} \text{Im} \left\langle\left\langle \hat{\rho}^{(0)}(t) \left| \frac{\partial \mathcal{L}}{\partial u_i(t)} \right| \hat{\rho}^{(1)}(t) \right\rangle\right\rangle, \quad (10)$$

where $\hat{\rho}^{(0)}(t)$ is a state backward-propagated with the conjugate Lindbladian, cf. (8), with the boundary condition

$$\hat{\rho}(T) = -\frac{\partial J_T}{\partial \langle\langle \rho(T) \rangle\rangle} = \hat{\rho}_{\text{tgt}}. \quad (11)$$

Only now is the update $\Delta u_i(t)$ discretized to a time grid ($\Delta u_i(t) \rightarrow \Delta u_{ij}$, $t \rightarrow t_j$), resulting in a formula that superficially resembles (7), with at least two crucial differences:

First, the forward-propagated state $\rho(t)$ uses the updated controls $u_i^{(1)}(t)$ in (10), and the guess controls $u_i^{(0)}(t)$ in (7). This makes Krotov's method *sequential* (updates at later times depend on updates at earlier times), whereas GRAPE is *concurrent* (updates are independent).

Second, the local derivative term in each equation differs; The gradient derivative $\partial \mathcal{E}_j / \partial u_{ij}$ can be evaluated similarly to \mathcal{E}_j itself, under the assumption that \mathcal{E}_j is a simple exponential [32]. In comparison, $\partial \mathcal{L} / \partial u_{ij} = [\hat{H}_i, \rho]$ is more straightforward to evaluate (and instantaneous).

The backward-propagated state $\hat{\rho}^{(0)}(t)$ is the same only for the specific functional (5); generally, in Krotov's method, it is determined by the boundary condition (11). Note that while we have assumed linear controls and a convex functional, Krotov's method can be also be extended to go beyond these assumptions [31].

2.3. Krotov's method for quantum trajectories

There are two possibilities for rewriting the optimization in terms of quantum trajectories. First, we can insert the expansion of $\hat{\rho}$ (2) into the functional (5) to find

$$J_T = 1 - \lim_{M \rightarrow \infty} \frac{1}{M} \sum_{k=1}^M \underbrace{|\langle \Psi_k(T) | \Psi_{\text{tgt}} \rangle|^2}_{\equiv \tau_k}. \quad (12)$$

That is, the fidelity is simply the average of the fidelities from each trajectory. We seek a single control that simultaneously implements the state-to-state transition for every $|\Psi_k\rangle$.

We now wish to ask, given the form of J_T , how the update rules for GRAPE and Krotov's method might be written in terms of the individual trajectories. For GRAPE this is not so simple; the form of the update rule is based on the fact that the evolution of $\hat{\rho}$ in each time step is given by the application of a linear operator \mathcal{E}_j , and this is no-longer true for the trajectories. Second, in a given time step the evolution of a given trajectory may contain one or more jumps at random times, which further complicates the calculation of the derivative with respect to the controls u_{ij} .

In contrast, for Krotov's method the functional (12) leads to the update equation [30]

$$\Delta u_i(t) = \frac{S_i(t)}{M\lambda_i} \sum_{k=1}^M \underbrace{\text{Im} \langle \chi_k^{(0)}(t) | \hat{H}_i | \Psi_k^{(1)}(t) \rangle}_{\equiv \Delta u_{ik}(t)}, \quad (13)$$

where $\chi_k^{(0)}(t)$ is backward-propagated with the boundary condition

$$\chi_k^{(0)}(T) = -\frac{\partial J_T}{\partial \langle \Psi_k |} = \tau_k^{(0)} | \Psi_{\text{tgt}} \rangle, \quad (14)$$

where $\tau_k^{(0)}$ is τ_k evaluated for the guess pulse. Since Krotov's method does not require the derivative of the time-evolution operator, this update equation is immediately compatible with the decomposition into quantum trajectories. Moreover, from a numerical perspective, the update equation can be evaluated with high efficiency: the contributions to $\Delta u_{ik}(t)$ to the update from every trajectory are completely independent. If the numerical method is parallelized, so that different trajectories are simulated on different processors, and a Message-Passing-Interface (MPI) is used for interprocessor communication, only these scalar values need to be communicated. We thus reap the full benefit of the MCWF method: reduction of the overall dimensionality by a factor of d , the dimension of the total Hilbert space. The required memory per node is reduced directly by that factor; the worst-case CPU time reduces by d^3 (as the fundamental operation in the time propagation is a matrix-vector multiplication).

We can obtain an alternative formulation of the control problem in terms of quantum trajectories by leaving the functional (5) in terms of the density matrix, and instead expanding the update equation in terms of the trajectories. For GRAPE this approach has the same issues as before, whereas for Krotov's method this results in the update equation

$$\Delta u_i(t) = \frac{S_i(t)}{M^2\lambda_i} \sum_{k,k'=1}^M \text{Im} \left[\langle \xi_k^{(0)}(t) | \hat{H}_i | \Psi_{k'}^{(1)}(t) \rangle \langle \Psi_{k'}^{(1)}(t) | \xi_k^{(0)}(t) \rangle \right], \quad (15)$$

using the decomposition

$$\hat{\mathbf{P}}^{(0)}(t) = \lim_{M \rightarrow \infty} \frac{1}{M} \sum_{k=1}^M |\xi_k\rangle \langle \xi_k| \quad (16)$$

for the backward-propagation with $|\xi_k(T)\rangle = |\Psi_{\text{tgt}}\rangle$. The above update now incorporates *cross-trajectory* information, including overlaps of the propagated states from each trajectory with those from every other trajectory. Compared to the full density matrix optimization, this alternative method maintains the saving in CPU time that comes from evolving the trajectories independently, but does incur significantly more communication overhead.

Both trajectory formulations of Krotov’s method, the “independent trajectory” and “cross-trajectory” formulations, guarantee monotonic convergence for $M \rightarrow \infty$. However, the numerical efficiency rests on the assumption that M can be kept reasonably small, ideally smaller than d (and certainly smaller than d^3). For a significantly larger number of trajectories, the total numerical resources will approach or even surpass those required for a full density matrix propagation. Note that even if there is no benefit in the *total* numerical resources, the memory *per compute node* is still reduced by a factor of d .

For finite (small) M , there is no guarantee of monotonic convergence. This is especially true because the stochastic jumps are different between iterations, as well as between the forward and the backward-propagation within the same iteration. Moreover, we expect the instantaneous jumps in the trajectory to cause jumps also in the control update. These jumps will average out both with the number of trajectories and the number of control iterations, but they may slow down convergence and may introduce noise into the optimized control field. To analyze how strongly the resulting optimized control fields are affected by these two factors, and to what extent the cross-trajectory update equation might be more robust, we now consider a practical example.

3. Creation of a single-excitation Dicke state in a quantum network

3.1. Network Model

We consider a network in which a number of “nodes” are connected via a traveling-wave field, depicted in Fig. 1. The nodes are connected to the field via circulators so that the field propagates from one node to the next in a single direction only, a configuration often referred to as a “cascade” network. Each node consists of a cavity containing a single atom. The atom encodes a qubit in two degenerate states $|g\rangle$, $|e\rangle$, driven via a Raman transition through an auxiliary level $|r\rangle$: $|g\rangle \leftrightarrow |r\rangle$ couples through a time-dependent drive $\Omega(t)$ with detuning Δ , while $|r\rangle \leftrightarrow |e\rangle$ is statically coupled with coupling strength g , see Fig. 1. For large Δ , the level $|r\rangle$ can be adiabatically eliminated [19], resulting in an effective two-level system whose coupling to the cavity is controlled via the drive $\Omega(t)$.

For a single node labeled (i) , the effective Hamiltonian in the rotating wave approximation then consists of drift term \hat{H}_0 and a driven Jaynes-Cummings term \hat{H}_d . With the cavity detuned from the driving field by g^2/Δ to compensate for the Stark shift, we find

$$\hat{H}^{(i)} = \hat{H}_0^{(i)} + \hat{H}_d^{(i)}, \quad (17)$$

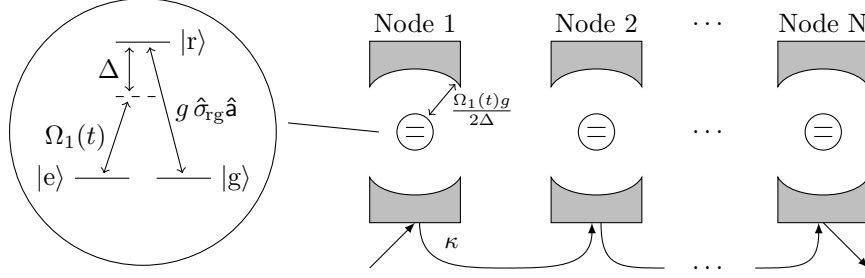


Figure 1. The structure of our network. A number of cavities, each containing a three-level atom in the Lambda configuration, are connected together by a traveling optical field that enters each cavity in turn via one of its end mirrors. Each cavity is coupled to the field via a circulator (not shown), so that the cavities only couple to field modes that are traveling from left to right. The field that is output from the first cavity thus enters the second, but not vice versa, in what is referred to as a “cascade” connection.

$$\hat{H}_0^{(i)} = -\frac{g^2}{\Delta} \hat{a}_i^\dagger \hat{a}_i + \frac{g^2}{\Delta} \hat{\Pi}_g^{(i)} \otimes \hat{a}_i^\dagger \hat{a}_i, \quad (18)$$

$$\hat{H}_d^{(i)} = -\frac{i\Omega_i(t)g}{2\Delta} \left(\hat{\sigma}_{e,g}^{(i)} \otimes \hat{a}_i - \text{c.c.} \right), \quad (19)$$

where \hat{a}_i is the cavity lowering operator, $\hat{\Pi}_g$ is the projector on the qubit ground state, and $\hat{\sigma}_{e,g}$ is the raising operator of the qubit. Leakage of photons out of the cavity is described by the Lindblad operator

$$\hat{L}^{(i)} = \sqrt{2\kappa} \hat{a}_i. \quad (20)$$

We now couple N cavities to a traveling-wave field via circulators, so that the field propagates from cavity to cavity in only one direction, as depicted in Fig. 1. The resulting master equation describing the evolution of all the cavities is obtained using input-output theory [8, 33, 9]. The explicit application of the theory is through the “SLH” formalism of Gough and James [7, 34, 35]. This formalism has been automated in the software package QNET ‡.

The total Hamiltonian is

$$\hat{H} = \sum_{i=1}^N \hat{H}^{(i)} + \sum_{i \neq j} \hat{H}^{(i,j)}, \quad (21)$$

$$\hat{H}^{(i,j)} = i\kappa \hat{a}_i^\dagger \hat{a}_j + \text{c.c.} \quad (22)$$

for the entire network. Note that the connection via the field yields the additional static interaction Hamiltonian $\hat{H}^{(i,j)}$ between *all* nodes of the network (not merely between nearest neighbors). The Lindblad operator for the entire network is

$$\hat{L} = \sum_{i=1}^N \hat{L}_i. \quad (23)$$

Thus, both the interaction between nodes, required to build entanglement, and the total dissipation of the network are proportional to the decay rate κ . However, the

‡ The python package QNET allows the user to construct quantum input-output networks, and will calculate the master equation for any such network [36].

form of the Lindblad operator allows for the individual summands $\hat{\mathcal{L}}_i$ to destructively interfere, canceling overall dissipation. If the dark-state condition [20, 21, 22, 23]

$$\forall t : \langle \Psi(t) | \hat{\mathcal{L}}^\dagger \hat{\mathcal{L}} | \Psi(t) \rangle = 0 \quad (24)$$

is fulfilled, an entangled state may be generated without loss of coherence.

3.2. Optimized creation of a single-excitation Dicke state

We assume that at time zero, the network is initialized in the state $|\Psi(t=0)\rangle = |eg\dots g\rangle$. That is, the atom in the cavity of the leftmost node is in the excited state, while all other nodes (and all cavities) are in the ground state. The state of the cavities, $|0\dots 0\rangle$ is implicit in our notation. We now seek the control fields $\Omega_i(t)$ (one field for each node) that will bring the system into an entangled Dicke state at a fixed final time T , $|\Psi(t=T)\rangle = \frac{1}{\sqrt{N}}(|eg\dots g\rangle + |ge\dots g\rangle + \dots + |gg\dots e\rangle)$. The cavity for all nodes again must be in the ground state at time T .

The optimization problem is solved by minimizing (5) using Krotov's method. We first do this optimization using the full density matrix, update (10), and then – for comparison – using a trajectory optimization, both for independent trajectories, functional (12) with update (13), and for the cross-trajectory method, update (15).

We are able to find optimized solutions for arbitrary N , limited numerically only by the exponential growth of the Hilbert space. As the Hamiltonian (21) preserves the total excitation in the system, it is sufficient to model both the cavity and the atom at each node as a two-level-system, resulting in a total Hilbert space dimension of 4^N . In principle, this makes the optimization numerically feasible up to $N = 4$ for density matrix optimization, and $N = 8$ for the trajectory methods.

However, for a succinct comparison between the methods, in the following we only consider the simplest case of $N = 2$ nodes, with control fields $\Omega_1(t)$ and $\Omega_2(t)$. In this case, the Dicke state is the Bell state

$$|\Psi\rangle_{\text{tgt}} = \frac{1}{\sqrt{2}}(|eg\rangle + |ge\rangle). \quad (25)$$

For full generality, we use a dimensionless Hamiltonian where energies are written in units of g . Consequently, time can be expressed in units of \hbar/g . For $\Delta = 100g$ and $\kappa = g$, through systematical variation of T , we find that the two-node Dicke state can comfortably be realized for $T = 5\hbar/g$. In general, the minimum time required to entangle the nodes of the network is proportional to the interaction Hamiltonian (22), that is, proportional to the value of κ .

Fig. 2 shows the result of an optimization starting from a simple Blackman-shaped guess pulse, see the dotted gray line in panel (a). For a direct density-matrix optimization using Krotov's method, that is the minimization of (5) with update (10), after 5000 iterations an error of $J_T = 1.3 \times 10^{-3}$ is achieved. The optimized pulses $\Omega_1(t)$ and $\Omega_2(t)$ for the first and second node are shown as the light blue and orange curves in Fig. 2(a). The corresponding dynamics are in panel (b), showing the smooth transition from the initial state $|eg\rangle$ to the superposition of $|eg\rangle$ and $|ge\rangle$: the excitation of the first and second qubit, the plotted expectation values $\langle \Pi_e^{(1)} \rangle$ and $\langle \Pi_e^{(2)} \rangle$, correspond directly to the population of $|eg\rangle$ and $|ge\rangle$, as the Hamiltonian preserves excitations ($\langle ee | ee \rangle \equiv 0$).

As the interaction between the nodes is mediated by photons being emitted from cavity 1 into cavity 2, both cavities are necessarily excited during the transition (see

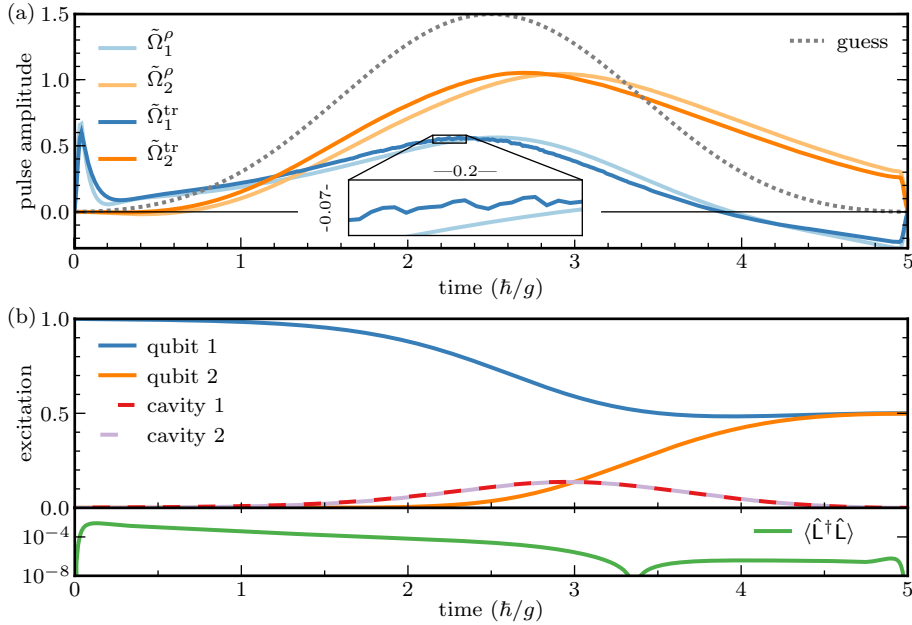


Figure 2. Optimized pulses and dynamics. (a) Optimized pulses for the creation of the Dicke state in a two-node network. $\tilde{\Omega}_{1,2}^\rho$ are the pulses for node 1, 2 resulting from optimizing using the density matrix. $\tilde{\Omega}_{1,2}^{\text{tr}}$ are the pulses from optimizing using two independent trajectories. All pulse amplitudes are normalized as $\tilde{\Omega}_{1,2}^{\rho,\text{tr}} \equiv \Omega_{1,2}^{\rho,\text{tr}}/2\Delta$. The guess pulse (identical for all nodes and optimizations) is indicated by the dotted gray curve. (b) Population dynamics under the optimized pulses $\tilde{\Omega}_i^\rho(t)$, as the expectation values of the qubit excitation, $\langle \hat{n}_e^{(i)} \rangle$, and the cavity excitation, $\langle \hat{a}_i^\dagger \hat{a}_i \rangle$, with $i = 1, 2$. In the bottom, the value of the dark-state condition (24).

the light and dark red dashed lines in Fig. 2(b)). Nonetheless, the dynamics are (nearly) coherent, due to the system being in a dark state (see the green line for $\langle \hat{L}^\dagger \hat{L} \rangle$ in the bottom of Fig. 2(b), which is close to zero). The two cavities are phase-shifted by π , that is $\langle \hat{a}_1 \rangle \approx -\langle \hat{a}_2 \rangle$, resulting in destructive interference for the total dissipator.

As we have not taken into account any other dissipation channels (such as spontaneous decay of the qubit), the deviation from the dark-state condition (24), is the only factor that limits the fidelity of the transfer. By continuing the optimization beyond 5000 iterations, the error could be made arbitrarily small in principle.

Optimizing with independent trajectories, and the cross-trajectory method, yields very similar results. As an example, the optimized pulses obtained from two independent trajectories, update (13), are shown as the dark blue and orange curves in Fig. 2(a). They are close, but not identical to the pulses obtained from direct density matrix optimization (lighter colored curves).

In general, running both optimization methods with differing numbers of trajectories, and the density matrix method, all yield comparable errors. Nevertheless there are differences in the rate of convergence, as well as in certain details of the pulse features. As shown in the zoomed inset of Fig. 2(a), there is some noise in the optimized pulses obtained from trajectory optimization, compared to the perfectly

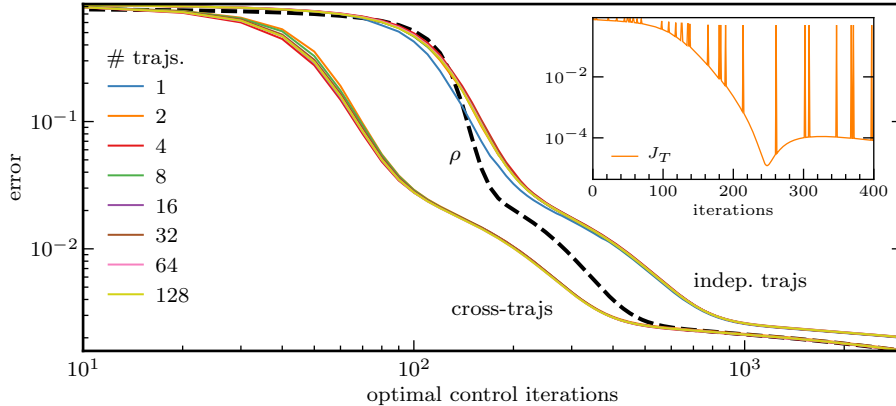


Figure 3. Comparison of convergence of optimization variants. For using between 1 and 128 independent trajectories, the error $1 - \langle\langle \hat{\rho}(T) | \hat{P}_{\text{tgt}} \rangle\rangle$ after each iteration (colored). This compares to the optimization using between 2 and 128 cross-trajectories, and the optimization directly in Liouville space (dashed black curve). All errors are evaluated from the exact density matrix evolution under the optimized pulses, which differs from the functional J_T actually guiding the optimization. For the example of an optimization using two independent trajectories, the value of J_T is shown in the inset.

smooth result of the density matrix optimization. This noise originates from the discontinuous jumps in the trajectories. In the following, we will analyze how both the convergence rate and the noise in the optimized pulses depend on the choice of optimization method and the number of trajectories.

3.3. Convergence of trajectory optimization

Fig. 3 shows the convergence, as measured by the error (5), over the number of iterations in the control procedure. In each iteration, the pulse is updated according to the appropriate update equation.

The convergence for the full density matrix optimization, update (10), is shown as the black dashed line. It compares to the convergence for using 1-128 independent trajectories (“indep. trajs”), update (13), and 2-128 cross-trajectories (“cross-trajs”), update (15). Remarkably, the number of trajectories (different colored lines), has almost no effect on the convergence. Thus, even a single trajectory can yield a satisfactory result, a significant reduction of numerical effort compared to the use of full density matrices.

After an initial plateau, the convergence when using independent trajectories lags behind the convergence for the full density matrix optimization. Asymptotically, the achieved error remains slightly higher. In contrast, when using cross-trajectories, the convergence is actually faster than the full density matrix, and asymptotically reaches the same error.

As the number of required trajectories again is small (even two trajectories are sufficient) it is worth pointing out that as long as the number of trajectories does not exceed the number of CPU cores available on a compute node, it would be easy to parallelize the method not using a message-passing interface, but instead using a shared-memory approach (e.g. OpenMP). In this case, the additional numerical

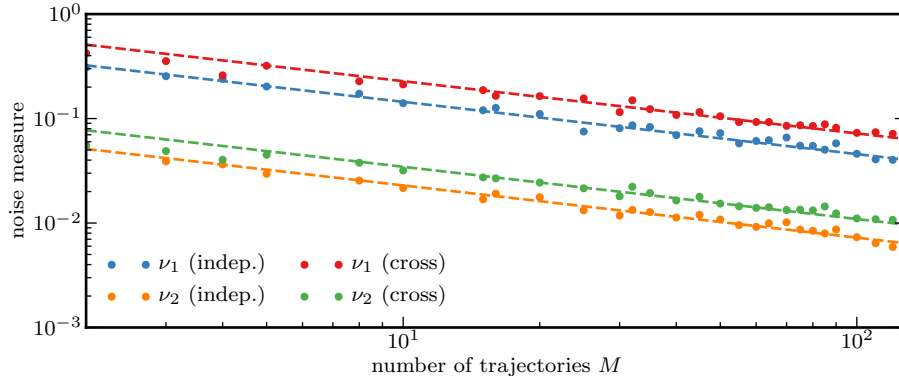


Figure 4. Scaling of noise artifacts in optimized pulses with the number of trajectories M . For both independent trajectories and cross-trajectory optimization, the noise measure according to (26) is shown for the pulse in each node. The dashed lines represent a fit to $\nu_i \propto 1/\sqrt{M}$

overhead of the cross-trajectory optimization relative to independent trajectories largely disappears.

For the optimizations using independent trajectories, the error (10) that is shown in Fig. 3 is not identical to the functional J_T that the optimization directly aims to minimize (12). Because of the finite number of trajectories and the randomness inherent in the quantum jumps, J_T itself does not converge monotonically. An example for two trajectories is shown in the inset of Fig. 3. The loss of a photon from the cavity (that is, a quantum jump) in a given iteration results in a total loss (error 1.0), as visible in the spikes in J_T . In addition, the lower envelope (J_T in the absence of photon loss) shows a local minimum around 250 iterations, owing to the two competing requirements of the optimization: achieving the desired target state (in the absence of photon loss), and minimizing decay (the dark-state condition). The non-monotonic convergence of J_T should not be held against the trajectory optimization method: as shown in Fig. 3 the actual physical error does decrease monotonically. For larger Hilbert spaces where a density matrix propagation is no longer feasible, we will generally not be able to analyze the convergence in terms of the true physical error, as it can only be determined from the propagation of $M \rightarrow \infty$ trajectories.

3.4. Jump noise

The use of trajectory optimization results in some noise in the control fields, cf. the inset in Fig. 2 (a). To analyze how the magnitude of this noise scales with the number of trajectories, we quantify the noise by comparing the optimized control field $\Omega_i(t)$ to a smoothed pulse $\Omega_i^{\text{smooth}}(t)$ obtained by applying a Savitzky-Golay filter [37] with a five-point cubic convolute (arbitrarily). We then define a noise measure

$$\nu_i = \int_0^T \left| \Omega_i(t) - \Omega_i^{\text{smooth}}(t) \right| dt \quad (26)$$

We find that this noise asymptotically scales with the number of trajectories M as $\nu_i \propto 1/\sqrt{M}$. This is illustrated in Fig. 4, which compares the noise measure for both pulses and for independent- and cross-trajectory optimization, for varying number of

trajectories M . The choice of window length and polynomial order in the smoothing filter only affects the proportionality factor, i.e. the y-intercept in Fig. 4.

For independent trajectories, the $1/\sqrt{M}$ scaling holds for all values of M . The pulse Ω_1 is noisier than the pulse Ω_2 , which is due to the fact that Ω_2 is closer to the original guess pulse than Ω_1 , see Fig. 2(a) – any noise induced by a jump is proportional to the magnitude of the pulse update in a given iteration.

The noise for the cross-trajectory optimization is systematically slightly higher than that for independent trajectories. We may conjecture that this is because the update (15) is quadratic in the (discontinuous) states, while the update (13) is only linear. However, for a small number of cross-trajectories ($< \approx 5$), the noise is smaller than the asymptotic $1/\sqrt{M}$ scaling, closer to the independent trajectories.

In any case, for this specific example, the noise has little effect on the fidelity, as we can see from Fig. 3: the optimization result is robust with respect to the level of noise introduced by the numerical procedure. If this were not that case, and if smooth pulses are required, one may also incorporate the smoothing directly into the optimization scheme by applying the Savitzky-Golay smoothing filter after each iteration (or after some fixed number of iterations).

4. Conclusion

We have formulated two variants of Krotov’s method of optimal control based on Monte-Carlo quantum jump trajectories for implementing state-to-state transitions.

The first variant considers M independent trajectories, and optimizes the target in each trajectory, averaging pulse updates from the trajectories. It is easily parallelized to M processes communicating with a message passing interface (MPI). The second “cross-trajectory” variant obtains an update by cross-referencing M trajectories into a coarse approximation of the density matrix evolution. When parallelized using MPI, this produces considerable overhead. However, for small M , a shared-memory parallelization model is efficient.

In any case, the use of trajectories provides a considerable numerical advantage for systems that are strongly dissipative, but for which simulating the full density matrix is not feasible due to the large dimension of the Hilbert space. In many cases, the memory to store a density matrix of size d^2 is not available, while a pure state of dimension d can easily be stored and propagated. This is typically the case for quantum networks, and we have illustrated the method for a simple example of creating an entangled Dicke state for a system of two cascaded cavities containing a trapped atom.

We find that the use of trajectories in the optimization yields results comparable to the full density matrix optimization. In the case of cross-trajectory optimization, the convergence of the optimization even outperforms the density matrix optimization.

Remarkably, the number of trajectories has almost no influence in the convergence or the error that is achieved. The number of trajectories does have an influence in the amount of noise artifacts in the optimized pulses that result from the discontinuous (jump) dynamics. These scale as $1/\sqrt{M}$ in the number of trajectories. At the same time, they have an only a negligible effect on the dynamics and the resulting error, and could also be removed by applying a smoothing filter to the optimized pulses.

Thus, we can conclude that a minimal number of trajectories (even just a single trajectory) is sufficient to optimize a state-to-state transition in a typical, highly dissipative system such as a quantum network. The method naturally extends to

optimization problems beyond a simple state preparation, e.g. the realization of quantum gates [38], or any other optimization that is easily expressed in terms of the density matrix. Also, instead of a quantum jump propagation, another trajectory method such as quantum state diffusion [24] could be used. In all cases, the feasibility of the optimization using Krotov's method results from the fact that no analytic derivative of the inherently non-analytical propagator is required.

Acknowledgments

The network model used in this paper was derived using the Python QNET package [36]. The propagation and optimization were done using the Fortran QDYN library [39]. The pulse smoothing was realized through SciPy's signal processing toolbox [40]. This research was supported in part by ASD(R&E) under their Quantum Science and Engineering Program (QSEP), and by the Army High Performance Computing Research Center (AHPARC) (sponsored by the U.S. Army Research Laboratory under contract No. W911NF-07-2-0027).

References

- [1] Blume-Kohout R, Caves C M and Deutsch I H 2002 *Found. Phys.* **32** 1641
- [2] Giovannetti V, Lloyd S and Maccone L 2011 *Nature Photon.* **5** 222–229
- [3] Stephens A M 2014 *Phys. Rev. A* **89**(2) 022321
- [4] Roy A and DiVincenzo D P 2017 Topological quantum computing *Topological Matter: Topological Insulators, Skyrmions and Majoranas, Lecture notes of the 48th IFF Spring School 2017* ed Bluegel S, Mokrusov Y, Schaeppers T and Ando Y p 278
- [5] Breuer H P and Petruccione F 2007 *The Theory of Open Quantum Systems* (Oxford: Oxford University Press)
- [6] Jacobs K 2014 *Quantum measurement theory and its applications* (Cambridge: Cambridge University Press)
- [7] Combes J, Kerckhoff J and Sarovar M 2017 *Adv. Phys. X* **2** 784–888
- [8] Gardiner C W and Collett M J 1985 *Phys. Rev. A* **31** 3761
- [9] Gardiner C W and Zoller P 2004 *Quantum Noise* (Springer)
- [10] Carmichael H 1993 *An Open Systems Approach to Quantum Optics* (Springer-Verlag, Berlin)
- [11] Diosi L 1986 *Phys. Lett. A* **114** 451
- [12] Wiseman H M 1996 *Quantum Semiclass. Opt.* **8** 205
- [13] Wiseman H M and Milburn G J 1993 *Phys. Rev. A* **47** 642
- [14] Hegerfeldt G C and Wilsner T S 1992 Ensemble or individual system, collapse or no collapse: A description of a single radiating atom *Classical and Quantum Systems, Proceedings of the Second International Wigner Symposium* ed Doebner H D, Scherer W and Schroeck F (Singapore: World Scientific) pp 104–115
- [15] Dum R, Zoller P and Ritsch H 1992 *Phys. Rev. A* **45** 4879
- [16] Mølmer K, Castin Y and Dalibard J 1993 *J. Opt. Soc. Am. B* **10** 524
- [17] Glaser S J, Boscain U, Calarco T, Koch C P, Köckenberger W, Kosloff R, Kuprov I, Luy B, Schirmer S, Schulte-Herbrüggen T, Sugny D and Wilhelm F K 2015 *Eur. Phys. J. D* **69** 279
- [18] Koch C P 2016 *J. Phys.: Condens. Matter* **28** 213001
- [19] Cirac J I, Zoller P, Kimble H J and Mabuchi H 1997 *Phys. Rev. Lett.* **78** 3221
- [20] Kraus B, Büchler H P, Diehl S, Kantian A, Micheli A and Zoller P 2008 *Phys. Rev. A* **78**(4) 042307
- [21] Clark S, Peng A, Gu M and Parkins S 2003 *Phys. Rev. Lett.* **91**(17) 177901
- [22] Cho J, Bose S and Kim M S 2011 *Phys. Rev. Lett.* **106**(2) 020504
- [23] Stannigel K, Rabl P and Zoller P 2012 *New J. Phys.* **14** 063014
- [24] Percival I 1998 *Quantum State Diffusion* (Cambridge University Press)
- [25] Plenio M B and Knight P L 1998 *Rev. Mod. Phys.* **70** 101
- [26] Khaneja N, Reiss T, Kehlet C, Schulte-Herbrüggen T and Glaser S J 2005 *J. Magnet. Res.* **172** 296
- [27] Byrd R H, Lu P, Nocedal J and Zhu C 1995 *SIAM J. Sci. Comput.* **16** 1190
- [28] Zhu C, Byrd R H, Lu P and Nocedal J 1997 *ACM Trans. Math. Softw.* **23** 550

- [29] Krotov V F 1996 *Global Methods in Optimal Control* (New York, NY, USA: Dekker)
- [30] Palao J P and Kosloff R 2003 *Phys. Rev. A* **68** 062308
- [31] Reich D M, Ndong M and Koch C P 2012 *J. Chem. Phys.* **136** 104103
- [32] de Fouquières P, Schirmer S, Glaser S and Kuprov I 2011 *J. Magnet. Res.* **212** 412
- [33] Gardiner C W 1993 *Phys. Rev. Lett.* **70**(15) 2269–2272
- [34] Gough J and James M 2009 *Commun. Math. Phys.* **287** 1109
- [35] Gough J and James M R 2009 *IEEE Transactions on Automatic Control* **54** 2530
- [36] <https://github.com/mabuchilab/QNET>
- [37] Savitzky A and Golay M J E 1964 *Anal. Chem.* **36** 1627
- [38] Goerz M H, Reich D M and Koch C P 2014 *New J. Phys.* **16** 055012
- [39] <https://qdyn-library.net>
- [40] Jones E, Oliphant T, Peterson P *et al.* SciPy: Open source scientific tools for Python
<http://www.scipy.org/>